Registration of 2D cardiac images to real-time 3D ultrasound volumes for 3D stress echocardiography

K. Y. Esther Leung[*a], Marijn van Stralen[a,b,c], Marco M. Voormolen[a,b], Gerard van Burken[a], Attila Nemes[a], Folkert J. ten Cate[a], Marcel L. Geleijnse[a], Nico de Jong[a,b], Antonius F. W. van der Steen[a,b], Johan H. C. Reiber[c], Johan G. Bosch[a]

[a]Thoraxcenter, Erasmus MC, Rotterdam, the Netherlands

[b]ICIN – Interuniversity Cardiology Institute of the Netherlands, Utrecht, the Netherlands

[c]Div. Image Processing, Dept. of Radiology, Leiden University Medical Center, Leiden, the Netherlands

ABSTRACT

Three-dimensional (3D) stress echocardiography is a novel technique for diagnosing cardiac dysfunction, by comparing wall motion of the left ventricle under different stages of stress. For quantitative comparison of this motion, it is essential to register the ultrasound data. We propose an intensity based rigid registration method to retrieve two-dimensional (2D) four-chamber (4C), two-chamber, and short-axis planes from the 3D data set acquired in the stress stage, using manually selected 2D planes in the rest stage as reference. The algorithm uses the Nelder-Mead simplex optimization to find the optimal transformation of one uniform scaling, three rotation, and three translation parameters. We compared registration using the SAD, SSD, and NCC metrics, performed on four resolution levels of a Gaussian pyramid. The registration's effectiveness was assessed by comparing the 3D positions of the registered apex and mitral valve midpoints and 4C direction with the manually selected results. The registration was tested on data from 20 patients. Best results were found using the NCC metric on data downsampled with factor two: mean registration errors were 8.1mm, 5.4mm, and 8.0° in the apex position, mitral valve position, and 4C direction respectively. The errors were close to the interobserver (7.1mm, 3.8mm, 7.4°) and intraobserver variability (5.2mm, 3.3mm, 7.0°), and better than the error before registration (9.4mm, 9.0mm, 9.9°). We demonstrated that the registration algorithm visually and quantitatively improves the alignment of rest and stress data sets, performing similar to manual alignment. This will improve automated analysis in 3D stress echocardiography.

Keywords: Three-dimensional ultrasound imaging, image registration, cardiovascular

1. INTRODUCTION

1.1. 3D Stress Echocardiography

Cardiovascular diseases are one of the major causes of death in the western world. Development of diagnostic techniques is therefore of great clinical importance. Stress Echocardiography is a commonly used, safe, and noninvasive technique that allows detection of myocardial dysfunction and of coronary artery disease [1]. Wall motion of the left ventricle (LV) is visualized with echocardiography in rest and under different levels of stress, induced by physical exercise or by pharmacological means. In classical two-dimensional (2D) stress echocardiography, standardized 2D cross-sections of the LV are imaged. Since acquisition in rest and stress stages are performed several minutes apart, the technique may suffer from variabilities in the visualized cross-sections. This may affect the accuracy of the wall motion comparison. With the emergence of real-time three-dimensional (3D) ultrasound [2, 3], new possibilities have arisen in dealing with such variabilities [4]. The whole LV can now be imaged, and true anatomical four-chamber (4C), two-chamber (2C), and short axis views can be generated afterwards in a more consistent manner. This should lead to more accurate comparison of cardiac wall motion in rest and stress.

[*] k.leung@erasmusmc.nl; phone +31 10 4638058; fax +31 10 4089445; http://www.erasmusmc.nl/ThoraxcenterBME/

Medical Imaging 2006: Image Processing, edited by Joseph M. Reinhardt, Josien P. W. Pluim,
Proc. of SPIE Vol. 6144, 614418, (2006) · 0277-786X/06/$15 · doi: 10.1117/12.652107

1.2. Registration

For comparison of LV wall motion under rest and stress conditions, it is essential that the ultrasound data are correctly aligned. Sources of misalignment are transducer movement between rest and stress acquisitions and patient respiration [5]. Therefore it is necessary to register the ultrasound volumes for a correct comparison of heart motion. Registration is a widely used technique for the alignment of two or more images. Registration of medical images is an active area of research. Overviews are given e.g. by Hill et al. [6] and Maintz and Viergever [7]. More recently, cardiac image registration methods have been reviewed by Mäkelä et al. [8]. Registration of ultrasound images has been explored by Rohling et al. [9], who registered 3D images of the gall bladder. Krücker et al. [10] used nonrigid registration for 3D spatial compounding of breast images. Roche et al. [11] used rigid registration to align intraoperative 3D ultrasound brain images with preoperative magnetic resonance images. Shekhar et al. [5] registered 3D images for stress echocardiography. They proposed rigid registration of full 3D volumes using mutual information, which was tested on ten patients. However, the method was only evaluated visually. In this work, we propose a registration algorithm based on 2D orthogonal image planes to 3D volumes, which will drastically reduce the computation effort. The algorithm is quantitatively validated and compared with inter- and intraobserver variabilities. Registration of 2D to 3D images is regularly used to find the correspondence between the operative scene and a preoperative image [12]. Registration of 2D interventional MR images to 3D preoperative MR images was investigated by Fei et al. [13]. Penney et al. [14] compared several similarity measures for 2D/3D registration of fluoroscopy and CT images. The registration algorithm in this work uses 2D four-chamber, two-chamber, and short axis images extracted from the 3D data set in the rest stage, which are then registered rigidly to the 3D image in the stress stage. Rigid registration is used to retrieve a global alignment of the anatomical coordinate system of both images.

1.3. Problem statement

It is the purpose of this study to develop a single modality registration algorithm for aligning the global anatomical coordinate system in rest and stress 3D ultrasound data sets. A method has been developed to manually extract four-chamber, two-chamber, and short-axis planes, which is used as gold standard. The registration and manual annotation methods are intended as a first step in automated analysis of stress echocardiography, but should also be useful for present clinical analysis. Differences in position in apex and mitral valve centre and differences in the 4C direction are used for quantitative evaluation. The registration is compared with inter- and intraobserver variabilities of the manual annotation.

2. METHODS

2.1. Data Acquisition

We acquired full-cycle 3D data sets from 20 patients, using a dobutamine stress protocol. The images used were obtained in the apical position. Three data sets were acquired with the Fast Rotating Ultrasound transducer [15], developed at the department of Biomedical Engineering (Thoraxcenter, Rotterdam, the Netherlands). The remaining 17 patients were examined using the Philips Sonos 7500 machine. The former produced voxel sets with spatial dimensions $128 \times 128 \times 388$, at a resolution of 1.4mm × 1.4mm × 0.3mm (length × width × depth); the latter had dimensions of $160 \times 144 \times 208$ voxels at a resolution of 1.1mm × 1.1mm × 0.7mm. Registration was tested on rest and stress pairs of 3D data sets at end-diastole (ED) and end-systole (ES). ED and ES volumes were chosen visually from the 4D data sets by selecting the time points of the ECG R-peak and mitral valve opening.

2.2. Plane Selection

We propose a new method of extracting the anatomical coordinate system in a 3D LV image, which is reminiscent of cardiac MR image planning protocols [16] and in agreement with current standards [17]. In each 3D volume, an orthogonal set of planes was manually selected, consisting of a four-chamber (4C) plane, a two-chamber (2C) plane, and

a short-axis plane constructed at 2/3 distance of the apex to the mitral valve. This procedure is also explained in the flowchart in Fig. 1. Since the z-axis of the 3D volume rarely coincides exactly with the LV long-axis, the long-axis was reconstructed iteratively as follows. The endocardial LV apex, defined as the highest point in the LV cavity, and two leaflet attachment points on the mitral valve ring were manually annotated in an initial vertical plane of the 3D data set. The new long-axis was taken as the line through the annotated 3D apex and the midpoint of the annulus. The plane transecting the estimated long-axis and normal to the initial vertical plane was then reconstructed, and the annotation was repeated. The idea is that by annotating the points iteratively, the indicated apex and mitral valve points will converge to the true positions. The annotation was repeated until the apex and mitral valve positions are correct in both orthogonal planes; this took typically four iterations. The method is illustrated for the apex in Fig. 2. Next, the direction of the four-chamber plane was determined by viewing several candidate long-axis planes 4° apart, 50° counter-clockwise from the aorta outflow tract at the mitral plane level, which was also manually selected. The 50° is chosen as an initial guess, but alternatively, the observer could manually indicate the desired direction in the mitral valve short-axis plane. The 4C plane was defined as passing through the long-axis and the centre of the tricuspid valve. An example of a manual annotation in an ED data set is given in Fig. 3.

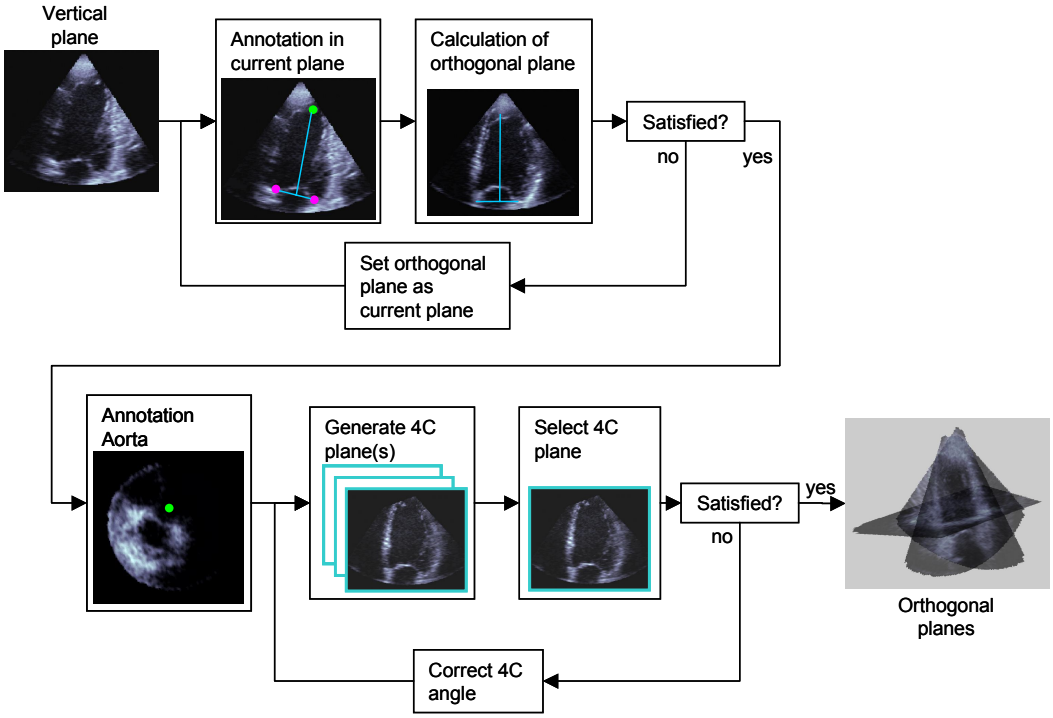

Fig. 1. Flow chart of the plane selection method. The apex and mitral valve are annotated iteratively in orthogonal vertical planes, until the long axis is in the correct position in both planes. The direction of the four-chamber plane was determined by viewing several long-axis planes 50°±4° counter-clockwise from the aorta outflow tract at the mitral plane level, which was also manually selected. Alternatively, the observer could manually indicate the 4C direction in the mitral valve short-axis plane. Orthogonal four-chamber, two-chamber, and short axis planes can then be constructed.

For the analysis of inter- and intra-observer variability, two independent observers manually selected the anatomical planes using the protocol described. The first observer annotated each data set twice, with a minimum interval of one day between the annotations. The second observer indicated 11 rest and 11 stress data sets twice, and the remaining data sets once. The averages over all observations (three to four observations per data set) for the annotated apex, mitral valve centre, and 4C direction were used to construct the orthogonal planes for the registration, providing a gold standard for the registration. The planes were interpolated tri-linearly on a grid of 0.7mm × 0.7mm, corresponding to the finest resolution of the Philips data sets. The intraobserver variability in the apex and mitral valve positions was defined as the Euclidean point distances in the two annotations per data set; the intraobserver variability in the 4C angle was

defined as the absolute difference in the manually selected 4C angle. Mean and standard deviations were calculated over all indicated data sets. The interobserver variability was defined in a similar manner, using the mean annotation of each observer in each data set.

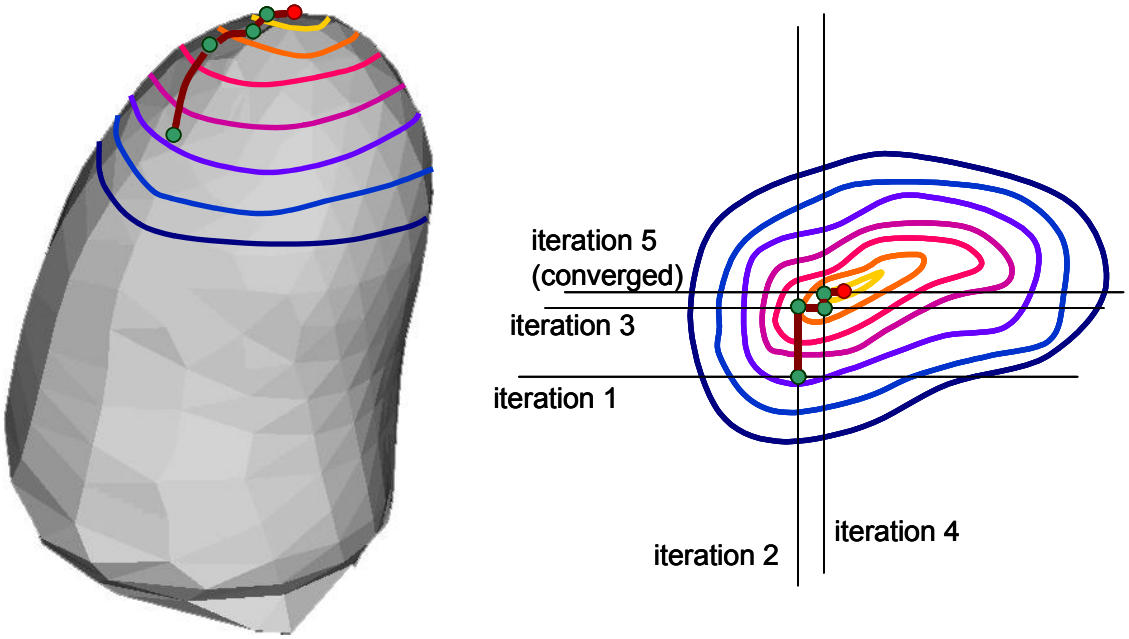

Fig. 2. Iterative annotation of the apex. Left: 3D schematic representation of the left ventricle with lines of constant altitude. Right: top view of the left ventricle. The apex is annotated iteratively as the highest point in orthogonal vertical planes, until the apex is at the highest point in both orthogonal views.

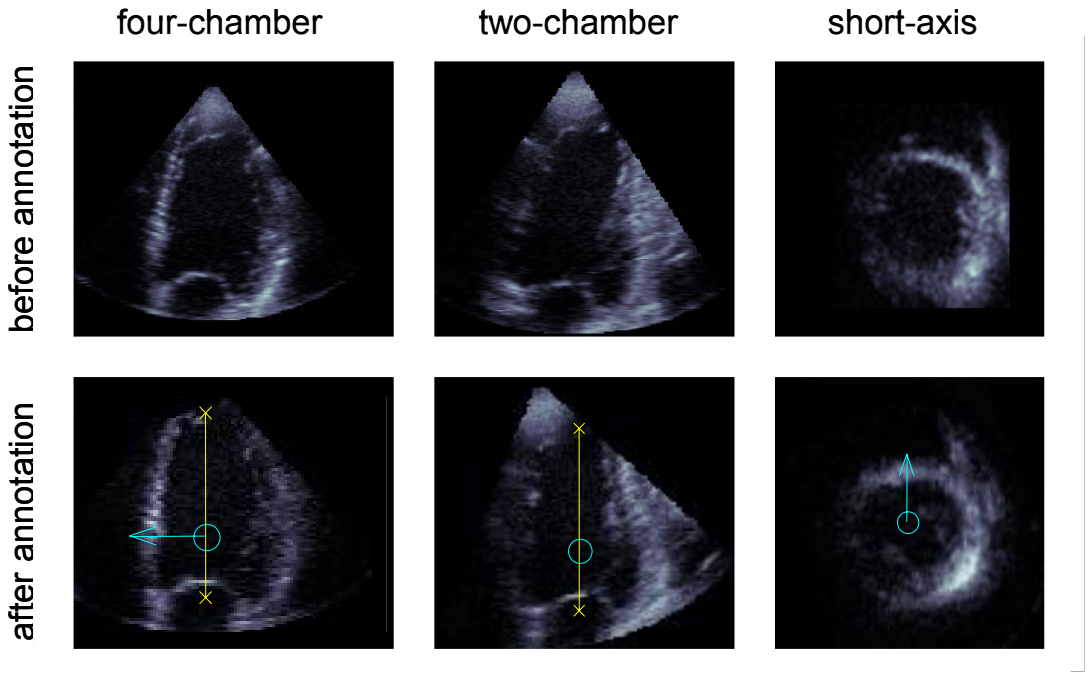

Fig. 3. Example of orthogonal four-chamber, two-chamber, and short axis planes selected from an ED volume.

2.3. Registration

The three planes in the rest stage acquisition were rigidly registered to the volume obtained in the stress stage using an intensity based registration approach. The optimal transformation of three rotations, three translations, and a uniform scaling factor was determined by the Nelder-Mead simplex optimization [18]. The parameter simplex was normalized according to the finest image resolution. One unit parameter corresponded to 1.1mm of translation, 0.4° rotation around the x- and y-axis, 0.5° rotation around the z-axis, and 0.7% scaling. The parameter units were chosen based on the physical displacement of the image voxel furthest away from the image origin. The origin of rotation coincided with the centre of the ultrasound transducer, thus correcting for probe tilting. The scaling was performed from the centre of the volume rather than from the rotation origin, thus preserving the shape of the LV as much as possible. The initial size of the simplex was 3 units along each parameter axis. Registration was considered converged if the simplex hypervolume was smaller than 0.01 unit parameter and if the metric value differences between the simplex vertices were less than 10^{-4}. The parameter simplex normalization was identical for all resolution levels.

As a second option, we also tested registration with a parameter simplex which varied with image resolution. The parameter simplex at level 0, the finest resolution level, was the same as described above. Then, at each successive level, the parameter simplex normalization doubled. For example, at level 1, one unit parameter corresponded to 2.2mm of translation, 0.8° rotation around the x- and y-axis, 1.0° rotation around the z-axis, and 1.4% scaling. This allowed the parameters to vary more freely at coarser resolution, to capture a larger range of motion.

We tested the sum-of-absolute-differences (SAD), sum-of-squared-differences (SSD), and normalized cross-correlation (NCC) metrics [19]. The registration was carried out on four resolution levels of a Gaussian pyramid [20], from full resolution at level 0 to 8 times downsampled at level 3. The background of the images was masked prior to registration. Trilinear interpolation was employed. Initial tests with one image registered to itself indicated that the capture range was approximately 10 parameter units (11mm translation, 4° to 5° rotation, and 7% scaling) at all resolutions, all parameters varied simultaneously.

Since twenty patients were considered and registration was performed in ED and ES, forty registrations were performed at each resolution level and for each metric. This amounted to $40\times4\times3 = 480$ registrations with the constant parameter simplex and $40\times3\times3 = 360$ registration with the varying parameter simplex, making a total of 840 registrations. Typical registration times of the algorithm, implemented in Matlab® (version 6.5.0, release 13, The Mathworks, Inc.) on a 2.8GHz Intel® Pentium® 4 processor were 13min., 3min., 30s, and 10s, for levels 0 through 4, respectively.

2.4. Validation method

Euclidean point distances of the apex and mitral valve positions, as well as the absolute differences in 4C angle, constitute the registration error. Registration errors are compared with the errors without registration, and tested for significance with the paired *t* test [21]. The registration errors are also compared with the inter- and intraobserver variability in the manual annotation of the data sets.

3. RESULTS

3.1. Visual assessment

Fig. 4 illustrates the registration results on an ES data set, on the finest resolution and with the NCC metric. The set of orthogonal 4C, 2C and short-axis planes of the reference rest stage is shown, along with the nonregistered stress planes, the results of registration, and the manually selected planes in the stress set. The registered stress set is better aligned than the nonregistered planes, and similar to the manually annotated set. Fig. 5 shows ED images of the rest data set, the nonregistered planes in the stress data set, and the results of registration with NCC at full resolution in checkerboard representation. The improvement in alignment can be perceived.

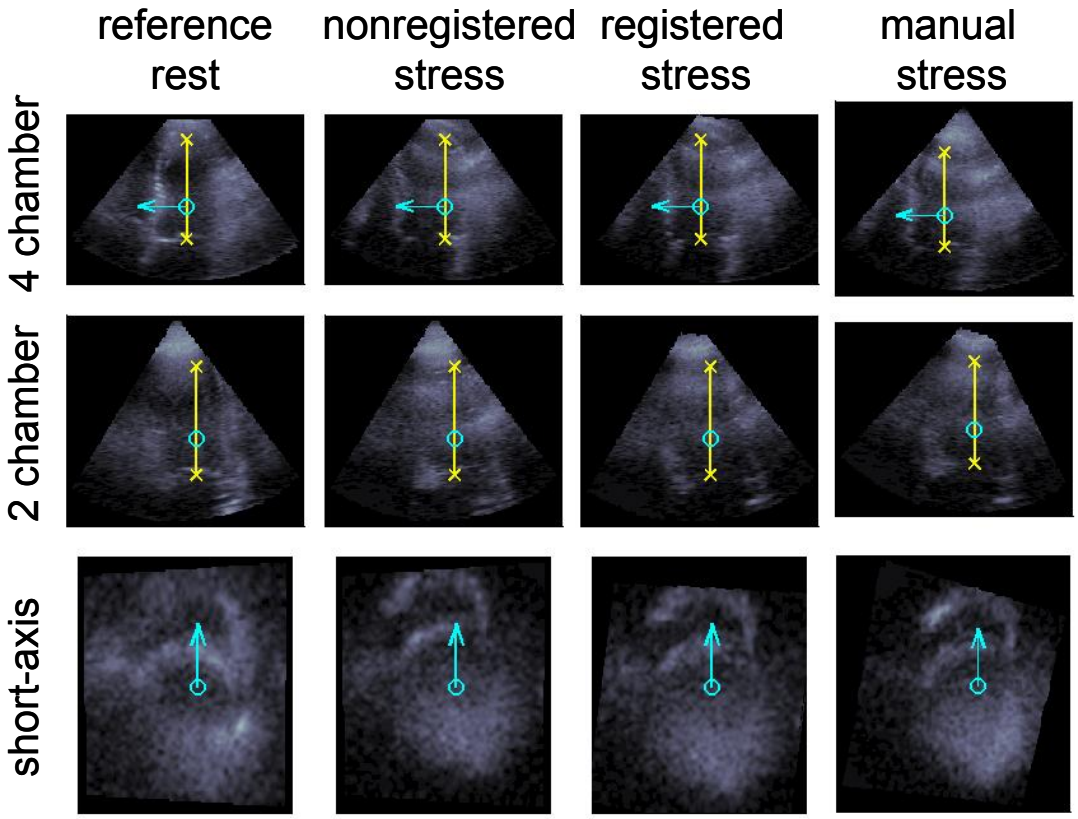

Fig. 4. Illustration of registration results, annotated. Set of orthogonal planes in end-systole: four chamber (top row), two chamber (middle row) and short-axis at 2/3 apex - mitral valve distance. Manually selected planes in rest stage acquisition were taken as reference (first column). The planes taken at the reference coordinates in the stress stage acquisition (second column) show misalignment in the apex, mitral valve and 4 chamber direction. The registration results using the NCC metric on full resolution data (third column) are in good agreement with the manually selected planes in the stress stage (fourth column).

3.2. Quantitative assessment

The registration algorithm was tested on four resolution levels and three different metrics were investigated. Better results were obtained when the parameter simplex was kept constant, than when the parameter simplex was allowed to vary across the different resolution levels. Best results were found using the NCC metric at resolution level 1, corresponding to twice downsampled data. In this case, all registration errors were significantly ($p<0.05$) lower than without registration. The results of the NCC metric for the four resolutions, using the constant parameter simplex, are given in Table I.

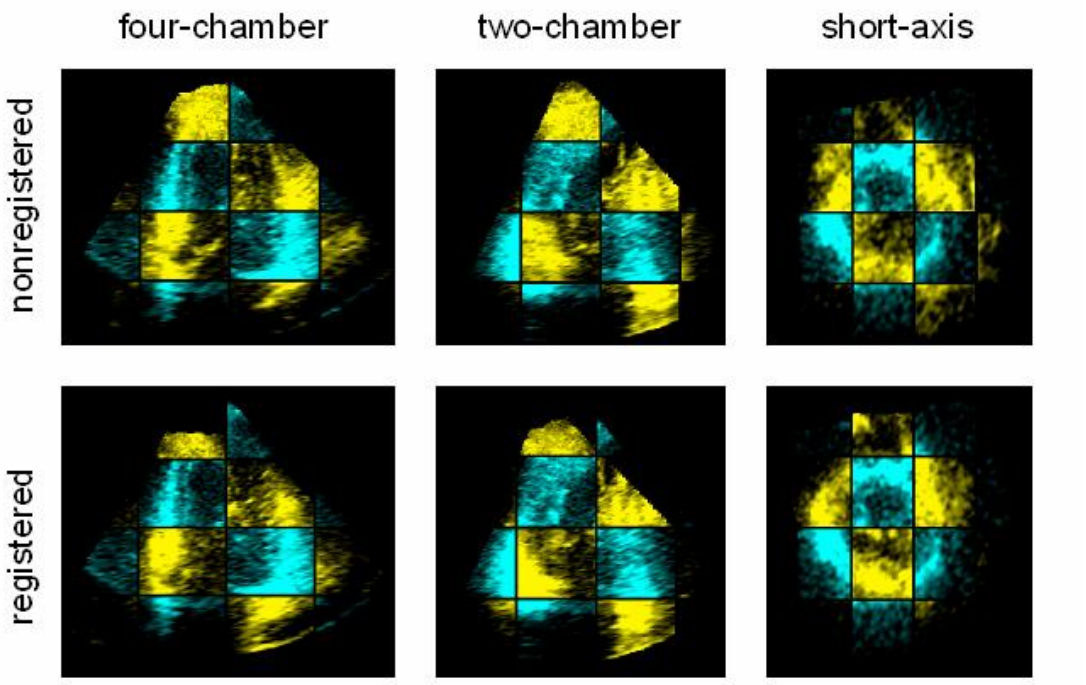

Fig. 5. Illustration of registration results in the checkerboard representation. Set of orthogonal four-chamber, two-chamber, and short-axis planes, without registration (top row) and after registration (bottom row). The (brighter) yellow patches are taken from the reference, rest stage data set. The cyan coloured patches correspond to the stress data set. Improvement in alignment after registration can be seen, especially in the two-chamber and short-axis views.

Table I: Summary of registration results for the NCC metric. Mean ± standard deviations of the errors are given. * denotes statistical significance (p<0.05) with respect to the error without registration.

	Registration error vs gold standard				Error without registra-tion	Inter-observer	Intra-observer
	level 0	level 1	level 2	level 3			
apex (mm)	7.7*±4.9	8.1*±5.8	9.2±5.7	10.7± 6.1	9.4±5.1	7.1±2.9	5.2±2.0
mitral valve (mm)	5.7*±4.9	5.4*±4.8	6.5*±5.4	8.0±5.8	9.0±4.0	3.8±1.3	3.3±1.5
4C direction (°)	8.4±4.8	8.0*±4.5	9.0±6.4	10.1±6.4	9.9±5.6	7.4±4.0	7.0± 3.5

Registration results using the constant parameter simplex are summarized in Fig. 6. The panels of the figure represent the mean error in apex position, mitral valve centre position, and direction of the 4C respectively. We see that the registration algorithm degrades when a coarser resolution was used, although the finest two levels perform similarly. At the coarsest level, results proved unsatisfactory for all metrics. As for the metrics, the NCC metric delivered considerably better alignment than SSD and SAD; the latter two metrics performed similarly. The registration gave smaller errors in the mitral valve position than the apex in all cases; also, the inter- and intraobserver variabilities are lower for the mitral valve annotation. As expected the intraobserver variabilities are lower than the interobserver.

Registration results using the parameter simplex which varied with image resolution are given in Fig. 7. The registration errors are now considerably higher than when using the constant parameter simplex (see Fig. 6). The best results in this case were obtained with NCC at full resolution, rather than resolution level 1.

We also examined the difference between registration in ED and ES. The results are shown for the NCC metric in Table II. The registration as well as the manual annotation is slightly better in ED than in ES.

Table II: Summary of registration results for the NCC metric, divided into ED and ES. Mean ± standard deviations are given.

Cardiac Phase		Mean registration error vs gold standard				Error without registration	Inter-observer	Intra-observer
		level 0	level 1	level 2	level 3			
ED	apex (mm)	7.4±4.7	7.9±5.3	8.6±4.9	9.9±5.8	9.3±5.4	7.8±3.1	4.8±1.6
	mitral valve (mm)	4.8±4.4	4.9±5.2	5.8±5.5	7.8±6.3	9.2±4.4	3.5±0.9	2.8±1.0
	4C direction (°)	8.0±5.0	7.7±5.0	8.9±7.8	9.9±7.5	9.2±5.2	7.4±4.8	6.4±2.9
ES	apex (mm)	8.0±5.2	8.3±6.4	9.8±6.4	11.6±6.4	9.5±5.0	6.4±2.7	5.5±2.4
	mitral valve (mm)	6.6±5.2	5.8±4.6	7.2±5.3	8.2±5.5	8.8±3.6	4.0±1.5	3.7±1.8
	4C direction (°)	8.8±4.7	8.2±4.1	9.0±4.8	10.4±5.3	10.7±6.1	7.3±3.2	7.5±4.1

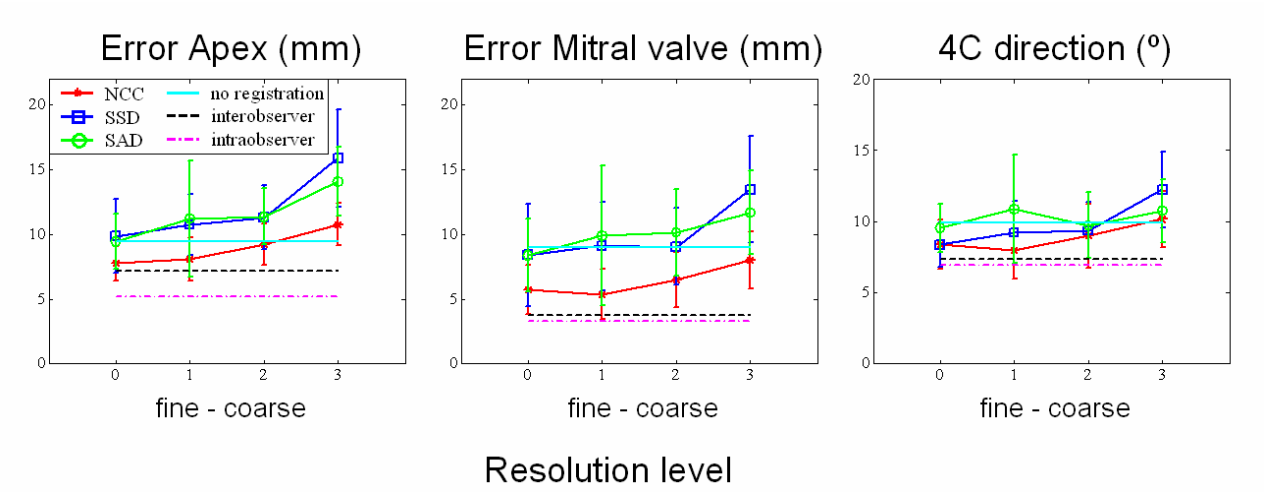

Fig. 6. Results of registration for the NCC, SSD, and SAD metric. The registration error of the apex position, mitral valve centre position, and four chamber (4C) direction is given, for four resolution levels. The errorbars correspond to 95% confidence intervals when tested against the nonregistered data. The interobserver and intraobserver variabilities, as well as the error without registration, are also given. Best results are obtained with the NCC metric. The registration performance degrades with resolution level.

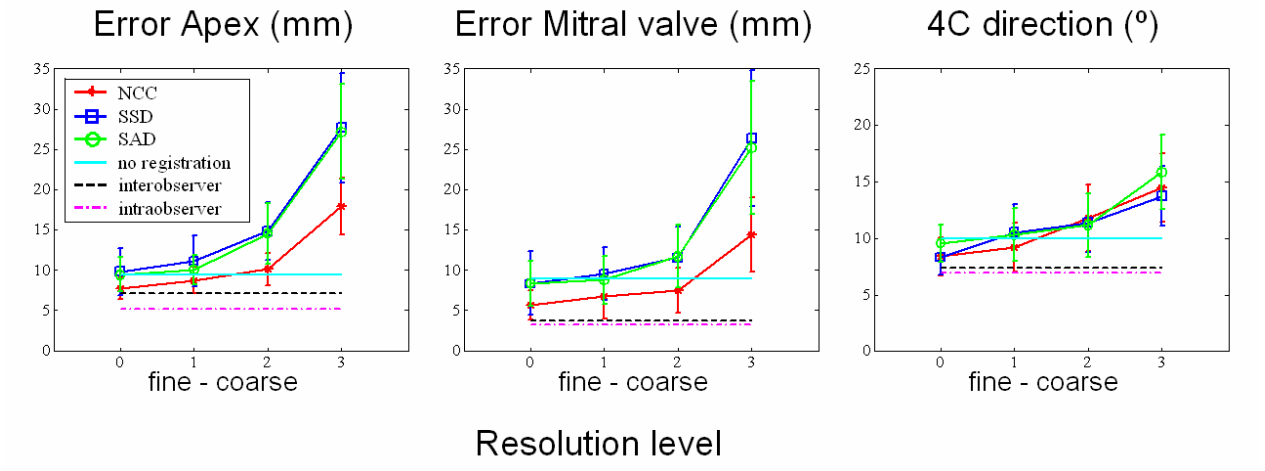

Fig. 7. Results of registration if the parameter simplex is varied with resolution, allowing more parameter variability as the resolution level increases. The errorbars correspond to 95% confidence intervals when tested against the nonregistered data. Registration errors of the apex position, mitral valve centre position, and four-chamber (4C) direction are shown for the NCC, SSD, and SAD metric. The interobserver and intraobserver variabilities, as well as the error without registration, are also given. Registration results degrade quickly as resolution level increases.

4. DISCUSSION

4.1. Registration algorithm

The registration algorithm with the NCC metric with twice downsampled data, using a constant parameter simplex, produces visually and quantitatively more aligned images, compared with the nonregistered results. The errors are close to manual intra- and inter-observer variability, and certainly below the errors made without registration. Given the poor image quality of some of the data sets, and considerable difference in appearance between rest and stress images, this is a promising result.

Best results were obtained at resolution level 1, rather than at full resolution. This may be due to Gaussian filtering at level 1, which removes speckle noise from the image while keeping global structures intact. At the coarsest resolution, where the data was downsampled with factor eight, most of these global structures have disappeared, making registration unfeasible.

In a multilevel approach, one might allow more freedom of movement in coarser resolution levels, and constrict transform parameter variation in finer levels. In our case, allowing more parameter variation by doubling the simplex normalization as described in the methods section, proved less effective. The starting misalignment of the images is rather small, since the sonographer checks the orientation of the heart during acquisition. With the varying simplex, the allowed parameter variation is too large, even at level 1, which causes the optimizer to search for solutions well outside of the possible parameter space, with the chance of converging to a local minimum.

Better results were obtained using the NCC metric, compared with SSD or SAD. The SAD and SSD assumes implicitly that the two images only differ by Gaussian noise [6], whereas the NCC makes a less strict assumption that there is a linear relationship between the intensity values in the images. Since ultrasonic image information is highly anisotropic and position dependent, this may be why NCC performs better than the other two metrics. This is especially true in our case, as the registration is not performed within the same image series but across different acquisitions.

The mitral valve could be registered more accurately than the apex, because the mitral valve is usually more clearly visible than the apex. Furthermore, the apex can be outside of the scan sector, or occluded by noise. Also, there were several cases where the LV showed signs of hyperkinesia. This is illustrated in Fig. 8. The heart is contracting excessively at the stress stage, so that the tissue around the apex is squeezed together. The observer could indicate the apex correctly, but since the registration algorithm only looks for global alignment, such details may be missed. As for the direction of the four-chamber plane, not much improvement can be obtained with registration. This may be because the orientation of the planes is checked by the sonographer during image acquisition. Also, the tricuspid valve may not always be clearly visible, making the 4C plane direction hard to define accurately.

The alignment of images in the ED cardiac phase was slightly better than in ES. This may be because the heart may suffer from contractility problems in the stress stage. At ES, when the LV contraction is at its peak, the relative stress-induced deformation of the LV may be larger than at ED, when the LV is relaxed. A rigid registration algorithm is then less accurate in calculating the alignment.

4.2. Future work

We plan to improve the registration method by investigating the parameters of the simplex optimization more thoroughly, and also trying other optimizers such as gradient descent and simulated annealing methods. Other metrics, e.g. mutual information, will allow registration of contrast-enhanced ultrasound images to images without contrast. Future work also consists in comparison of 2D stress echo images with registered images in the 3D data set, to

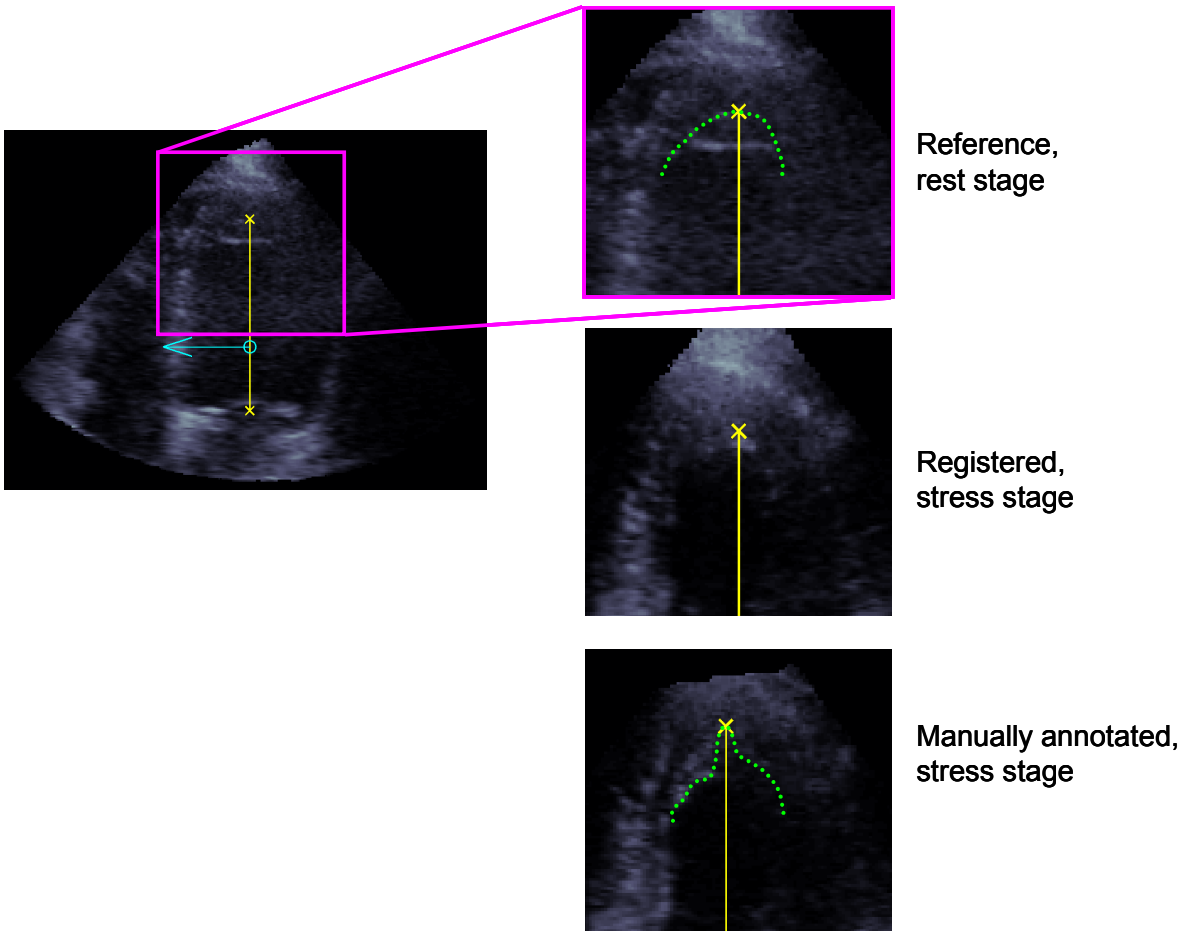

Fig. 8. Example where rigid registration fails. At stress, the left ventricle (LV) may contract excessively as in this case. The LV wall is squeezed in the region of the apex, so that the endocardial border at the apex location changes shape dramatically. Rigid registration, which searches for global alignment, cannot detect such details.

investigate the improvement of novel 3D stress echocardiography compared with the traditional 2D technique. We would like to extend the method to cope with time series and generalized registration of model to patient.

5. CONCLUSION

An intensity based rigid registration algorithm has been developed to extract 2D four-chamber, two-chamber, and short-axis planes from 3D images acquired in stress echocardiography. Optimal alignment is obtained with the NCC metric at twice downsampled data. The registration algorithm produces visually and quantitatively more aligned images, compared with the nonregistered results. The errors are close to manual intra- and inter-observer variability, and certainly below the errors made without registration. This will aid automated analysis in 3D stress echocardiography.

ACKNOWLEDGMENTS

Financial support from the Dutch Technology Foundation STW (Grant LGT 6666) is gratefully acknowledged. The authors also thank Mike Danilouchkine for the useful discussions.

REFERENCES

1. T. H. Marwick, *Stress echocardiography: its role in the diagnosis and evaluation of coronary artery disease*, 2nd ed. Norwell, Massachusetts: Kluwer Academic Publishers, 2003.
2. J. A. Panza, "Real-time three-dimensional echocardiography: an overview," *Int. J. Cardiovas. Imag.*, vol. 17, pp. 227-235, 2001.
3. R. S. von Bardeleben, H. P. Kühl, S. Mohr-Kahaly, and A. Franke, "Second-generation real-time three-dimensional echocardiography: finally on its way into clinical cardiology?," *Z. Kardiol.*, vol. 93: Suppl 4, pp. IV/56 - IV/64, 2004.
4. M. Ahmad, T. Xie, M. McCulloch, G. Abreo, and M. Runge, "Real-time three-dimensional dobutamine stress echocardiography in assessment of ischemia: comparison with two-dimensional dobutamine stress echocardiography," *J. Am. Coll. Cardiol.*, vol. 37, pp. 1303-1309, 2001.
5. R. Shekhar, V. Zagrodsky, M. J. Garcia, and J. D. Thomas, "Registration of real-time 3-D ultrasound images of the heart for novel 3-D stress echocardiography," *IEEE Trans. Med. Imag.*, vol. 23, pp. 1141-1149, 2004.
6. D. L. G. Hill, P. G. Batchelor, M. H. Holden, and D. J. Hawkes, "Medical image registration," *Phys. Med. Biol.*, vol. 46, pp. 1-45, 2001.
7. J. B. A. Maintz and M. A. Viergever, "A survey of medical image registration," *Med. Image Anal.*, vol. 2, pp. 1-36, 1998.
8. T. Mäkelä, P. Clarysse, O. Sipilä, N. Pauna, Q. C. Pham, T. Katila, and I. E. Magnin, "A review of cardiac image registration methods," *IEEE Trans. Med. Imag.*, vol. 21, pp. 1011-1021, 2002.
9. R. N. Rohling, A. H. Gee, and L. Berman, "Automatic registration of 3-D ultrasound images," *Ultrasound Med. Biol.*, vol. 24, pp. 841-854, 1998.
10. J. F. Krücker, C. R. Meyer, G. L. LeCarpentier, J. B. Fowlkes, and P. L. Carson, "3D Spatial Compounding of Ultrasound Images using Image-Based Nonrigid Registration," *Ultrasound Med. Biol.*, vol. 26, pp. 1475-1488, 2000.
11. A. Roche, X. Pennec, G. Malandain, and N. Ayache, "Rigid registration of 3-D ultrasound with MR images: a new approach combining intensity and gradient information," *IEEE Trans. Med. Imag.*, vol. 20, pp. 1038-1049, 2001.
12. J. P. Pluim, J. B. Maintz, and M. A. Viergever, "Mutual-information-based registration of medical images: a survey," *IEEE Trans. Med. Imag.*, vol. 22, pp. 986-1004, 2003.
13. B. Fei, J. L. Duerk, D. T. Boll, J. S. Lewin, and D. L. Wilson, "Slice-to-Volume Registration and its Potential Application to Interventional MRI-Guided Radio-Frequency Thermal Ablation of Prostate Cancer," *IEEE Trans. Med. Imag.*, vol. 22, pp. 515-525, 2003.
14. G. P. Penney, J. Weese, J. A. Little, P. Desmedt, D. L. G. Hill, and D. J. Hawkes, "A comparison of similarity measures for use in 2-D - 3-D medical image registration," *IEEE Trans. Med. Imag.*, vol. 17, pp. 586-595, 1998.
15. M. M. Voormolen, B. J. Krenning, C. T. Lancee, F. J. ten Cate, J. R. T. C. Roelandt, A. F. W. van der Steen, and N. de Jong, "Harmonic 3D echocardiography with a fast rotating ultrasound transducer," *IEEE Trans. Ultrason. Ferroelectr. Freq. Control, accepted*.
16. B. P. F. Lelieveldt, R. J. van der Geest, H. J. Lamb, H. W. M. Kayser, and J. H. C. Reiber, "Automated observer-independent acquisition of cardiac short-axis MR images: a pilot study," *Radiology*, vol. 221, pp. 537-542, 2001.
17. M. D. Cerqueira, N. J. Weissman, V. Dilsizian, A. K. Jacobs, S. Kaul, W. K. Laskey, D. J. Pennell, J. A. Rumberger, T. Ryan, and M. Verani, "Standardized myocardial segmentation and nomenclature for tomographic imaging of the heart," *Circulation*, vol. 105, pp. 539-542, 2002.
18. J. C. Lagarias, J. A. Reeds, M. H. Wright, and P. E. Wright, "Convergence properties of the Nelder-Mead simplex method in low dimensions," *SIAM J. Optim.*, vol. 9, pp. 112-147, 1998.
19. A. Giachetti, "Matching techniques to compute image motion," *Image Vision Comput.*, vol. 18, pp. 247-260, 2000.
20. P. J. Burt and E. H. Adelson, "The Laplacian pyramid as a compact image code," *IEEE Trans. Commun.*, vol. COM-31, pp. 532-540, 1983.
21. D. G. Altman, *Practical statistics for medical research*, 1st ed. London: Chapman and Hall, 1997.